Nitric Oxide 82 (2019) 12–24

Contents lists available at ScienceDirect

Nitric Oxide

journal homepage: www.elsevier.com/locate/yniox

Inhibition of JNK and activation of the AMPK-Nrf2 axis by corosolic acid suppress osteolysis and oxidative stress

Mingzheng Peng[a], Lei Qiang[b], Yan Xu[b], Cuidi Li[c], Tao Li[a], Jinwu Wang[a,*]

[a] Shanghai Key Laboratory of Orthopaedic Implant, Department of Orthopaedic Surgery, Shanghai Ninth People's Hospital, Shanghai Jiao Tong University School of Medicine, 639 Zhizaoju Rd, Shanghai, 200011, China
[b] Southwest Jiaotong University College of Medicine, 610031, No.111, North Section, 2nd Ring Road, Chengdu, Sichuan, China
[c] Med-X Research Institute, School of Biomedical Engineering, Shanghai Jiao Tong University, 1804 Huashan Rd, Shanghai, 200030, China

ARTICLE INFO

Keywords:
Corosolic acid
AMPK
Osteoclastogenesis
Nrf2
Reactive oxygen species

ABSTRACT

The intracellular reactive oxygen species contribute to RANKL-induced osteoclastogenesis and osteolysis. Nuclear factor-erythroid 2-related factor 2 (Nrf2), a redox-sensitive transcription factor, is critical in the cellular defense against oxidative stress by induction of antioxidants and cytoprotective enzymes. In the current study, it was first demonstrated that RANKL-induced osteoclastogenesis and hydroxylapatite resorption were suppressed by Corosolic acid (CA) via inhibiting p-JNK and activating p-AMPK. Meanwhile, p-65, p-38, Akt, and GSK-3β were partly inhibited during the treatment of CA. Osteoclastogenesis related genes, including NFATc1, c-fos, cathepsin K, and CTR were down-regulated by CA as well. Furthermore, the intracellular oxidative stress of CA-treated osteoclasts was dramatically decreased and Nrf2 was translocated into the nucleus to activate antioxidants including HO-1, NQO-1, and GCLC by CA. The LPS-induced mice calvarial osteolysis model was established for the in vivo investigation. Micro-CT morphometric analysis revealed that the treatment of CA restored LPS-induced bone loss and formation of osteoclasts. Besides, p-p65 and p-JNK were activated in the LPS group but inhibited by CA in vivo. The treatment of CA also activated p-AMPK during its attenuating LPS-induced osteolysis. Conclusively, CA effectively protects against LPS-induced osteolysis by suppressing osteoclastogenesis and oxidative stress through the inhibition of the JNK and activation of the AMPK-Nrf2 axis.

1. Introduction

Bone contains multiple cytokines, cells and secreted matrixes [1,2]. Osteoclasts, one kind of multiple nucleus giant cells that formed from bone marrow or peripheral blood-derived monocytes, play a pivotal role in turnover and homeostasis of bone by decomposing and resorbing bone matrix working with bone-forming osteoblasts [3]. Therefore, the abnormality of differentiation and function of osteoclasts lead to many diseases including osteoporosis and osteoarthritis. Recently, many effective drugs targeting at osteoclastogenesis have been demonstrated as owning bone protective and repairing properties [4–6]. In osteoclastogenesis, the osteoblasts-secreted RANKL binds to its receptor RANK on monocytes to active TRAF6, which phosphorylates the downstream kinases such as NF-κB and Mitogen-activated protein kinase (MAPK). Activation of NF-κB and MAPK up-regulates the expression of osteoclast-associated transcription factors such as c-Fos and NFATc1, resulting in differentiation and maturation of osteoclasts [7,8].

Reactive oxygen species (ROS) is an important regulator of bone cell function and plays an important role in the maintenance of bone homeostasis. Thus, maintaining the balance of oxidation and antioxidant systems or ROS-targeted antioxidants can be used as the treatment or prevention of bone diseases including osteoporosis. The binding of RANKL to its receptor RANK and increases intracellular ROS levels by activating TRAF6, NOX1 and RAC1 [9]. It was demonstrated that ROS possesses deleterious effects on cells including peroxidation of lipids and phospholipids, and oxidative damage to proteins and DNA [10,11]. Therefore, cells have several protective mechanisms against these oxidative stressors [12,13]. Nuclear factor-erythroid 2-related factor 2 (Nrf2) is the key transcription factor that regulates the generation of cytoprotective antioxidants including cytoprotective enzymes including heme oxygenase-1 (HO-1), NAD(P)H: quinone reductase (NQO-1), γ-glutamylcysteine synthetase catalytic subunit (GCLC) and modifier subunit (GCLM), all of which are ROS scavengers [14,15]. AMP-activated protein kinase (AMPK) has also been demonstrated to be a critical factor in oxidative response, inflammation, and tumorigenesis [16–18].

* Corresponding author.
E-mail address: Jinwu_wang@163.com (J. Wang).

https://doi.org/10.1016/j.niox.2018.11.002
Received 31 August 2018; Received in revised form 6 October 2018; Accepted 15 November 2018
Available online 16 November 2018
1089-8603/ © 2018 Elsevier Inc. All rights reserved.

Plant-derived natural products are gaining more importance for the treatment of osteoporosis. Previous reports have also identified that various natural products including Carnosic acid, Avenanthramides, and Sodium hydrosulfide, were found to effectively inhibit osteoclast differentiation to prevent excessive bone resorption by inducing Nrf2/HO-1, and eliminate ROS and oxidative stress in osteoclasts [19,20]. Corosolic Acid (CA) was first reported by Ahn et al., in 1998 that it was a triterpenoid extracted from *A. valvata Dunn and Lagerstroemia speciosa* L, which displayed anti-cancer activity and suppresive activity against protein kinsae C (PKC) [21]. CA has also been reported as own anti-oxidants, anti-inflammatory, anti-tumor properties [22,23]. Nevertheless, the effect of CA on osteoclastogenesis and LPS-induced osteolysis remains unknown.

In the present study, we investigated the effect of CA on the generation of intracellular ROS and RANKL-induced oxidative stress within osteoclasts. Our results demonstrated that CA inhibited osteoclastogenesis by suppressing NF-kB and MAPK as well as activating AMPK and Nrf2 resulting in up-regulation of antioxidants in vitro and attenuated LPS-induced osteolysis in vivo.

2. Materials and methods

2.1. Reagents

Corosolic acid (purity, > 98%, as determined by high-performance liquid chromatography) was purchased from MeilunBio Co. (Dalian, Liaoning, China). Recombinant mouse cytokines were purchased from R&D Systems (Minneapolis, MN, USA). All antibodies were purchased from Cell Signaling Technology or Abcam. Special hydroxyapatite-coated plates were purchased from Corning Life Science (St. Lowell, MA, USA). Compound C (Dorsomorphin), Anisomycin and Brusatol were used as the inhibitor of p-AMPK, activator of p-JNK and inhibitor of Nrf2, respectively, which were purchased from MeilunBio Co. (Dalian, Liaoning, China).

2.2. Isolation of mouse bone marrow-derived monocytes (BMMs) and cell culture

All experimental protocols were approved by the Ethics Committee of Shanghai Ninth People's Hospital (Shanghai, China), which abide by the guidelines and procedures of the Animal Care and Use Committee of Shanghai Jiao Tong University School of Medicine. As reported before, BMMs of C57BL/6 mice and RAW 264.7 cell lines were used as osteoclasts precursors [24].

2.3. Cell viability assay

The effect of CA on cell proliferation was detected using CCK-8 along with the manufacturer's instructions. In brief, BMMs and RAW 264.7 cells were inoculated into 96-well plates with sextuplicate simples. After cells attached, culture media were replaced with ones containing 0, 10, 20, 40, 80, 160, or 320 μM CA for incubation 24, 48, 72, or 96 h. At each time points, old culture media were discarded and serum-free media with 10% CCK-8 solution followed by incubation of 2 h at 37 °C, 5% CO2 without light. Next, the absorbance was detected with a Bio-Tek Synergy HT spectrophotometer at 450 nm.

2.4. In vitro osteoclastogenesis assay

For inducing osteoclastogenesis in vitro, we inoculated appropriate number of BMMs in 96-well plates, 24-well plates, or confocal dishes, and incubated them with complete culture media containing 30 ng/ml M-CSF, 50 ng/ml RANKL, and 0, 5, or 10 μM CA. The mature osteoclasts, multiple nucleus giant cells (MNCs), were recognized as positive TRAP staining cells with more than 3 nuclei. Meanwhile, the average number of osteoclasts and percentage of the TRAP-positive stained area were both calculated using Image-Pro Plus 6.0 from five random 100 × magnified views for each group.

Table 1
The mouse primer sequences of osteoclastogenesis marker genes for RT-PCR.

Gene	Forward Sequence	Reverse Sequence
NFATc1	TTGAGCTGAGGAAAGGGGAG	TGACTGGGTAGCTGTCTGTG
C-Fos	AGAAACACGTCTTCCCTCGA	TTGCCAGGAACACAGTAGGT
cathepsin K	ACTCCAGTCAAGAACCAGGG	CAACTTTCATCCTGGCCCAC
CTR	TGCAGACAACTCTTGGTTGG	TCGGTTTCTTCT CCTCTGGA
COX-2	ACACACTCTATCACTGGCACC	TTCAGGGCGAAGCGTTTGC
iNOS	ACATCGACCCGTCCACAGTAT	CAGAGGGGTAGGCTTGTCTC
GAPDH	ACCCAGAAGACTGTGGATGG	CACATTGGG GGTAGGAACAC

F-actin rings formed in osteoclasts were detected as well. After induced by M-CSF and RANKL for 5 days, cells were fixed with 4% paraformaldehyde for 30 min before permeabilized by 0.1% Triton-100 for 5min. Then cells were subsequently stained and incubated with rhodamine-conjugated phalloidin (1:100; Invitrogen Life Technologies, Carlsbad, CA, USA) and DAPI for 30 min and 5 min respectively after blocked by 10% bovine serum albumin for 1 h. Afterward, the F-actin rings were observed under a confocal fluorescent microscope.

For evaluating the effect of CA on hydroxylapatite resorption of osteoclasts, special hydroxylapatite-coated 24-well plates provided by Corning Inc (#3987; NY, USA) were used as above descriptions. After osteoclasts were induced for 10 days with or without CA, the cells were gently digested with trypsin and the plates were carefully washed with PBS, followed by Von Kossa stain to distinguish the resorbed pits. The average number of resorbed pits and the percentage of the resorbed area were both calculated.

2.5. Enzyme-linked immunosorbent assay (ELISA)

The secretions of several inflammatory cytokines including IL-1β, TNF-α, and IL-6 were detected by ELISA. The samples were extracted from the culture supernatant of macrophages stimulated by LPS with or without the treatment of 0, 5, or 10 μM CA. Three independent experiments were repeated.

2.6. Reactive oxygen species (ROS) assay

For measuring the amount of ROS within osteoclasts, we used dichlorofluorescein diacetate (DCFH-DA) and Oxiselect™ Intracellular ROS assay kit (Cell Biolabs, Inc., San Diego, CA, USA) according to the manufacturer's instructions. In brief, 6×10^5 per well BMMs were inoculated at 6-well plates and induced by 30 ng/ml M-CSF and 50 ng/ml RANKL with or without the treatment of CA. 24 h later, a final concentration of 10 μmol/l DCFH-DA was added into all groups. The produced intracellular ROS converted the non-fluorescent DCFH into fluorescent DCFH-DA, which was detected by a Bio-Tek Synergy HT spectrophotometer.

2.7. Nrf2-ARE-luciferase assay

Nrf2-ARE-luciferase reporter gene transfected RAW 264.7 cells were constructed as previous descriptions [25,26]. In brief, 2×10^5 RAW 264.7 cells were inoculated in 24-well plates and cultured with or without CA for 6 h, followed by stimulation of 100 ng/ml RANKL for 8 h. After the cells were lysed with luciferase lysis buffer, luciferase activity was detected using a Luciferase Assay Kit (Promega, Madison, WI, USA).

2.8. Total RNA extraction and real-time polymerase chain reaction (RT-PCR)

Quantitative PCR was used to measure the expression of specific

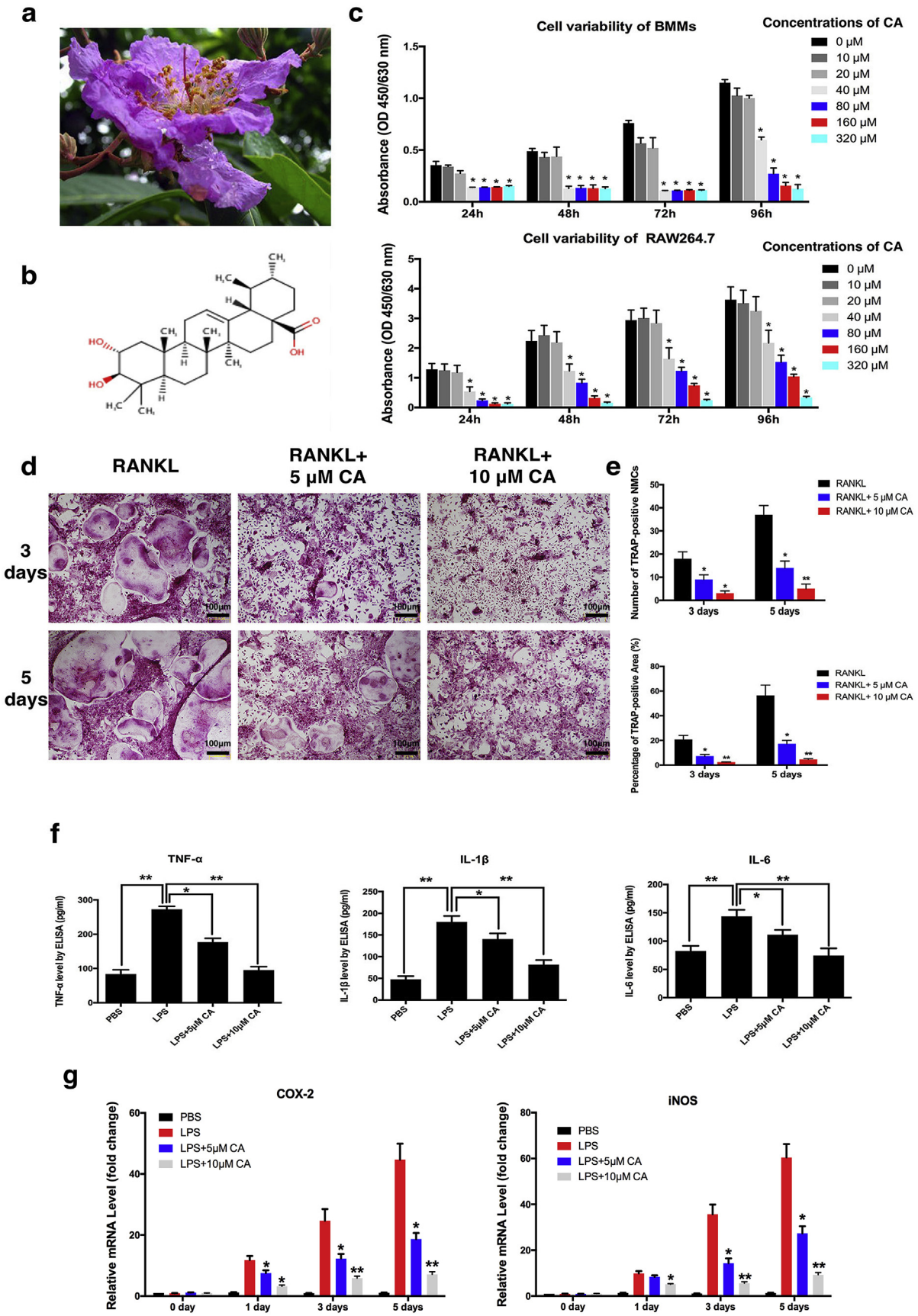

Fig. 1. CA inhibited RANKL-induced osteoclastogenesis in vitro. (a) natural form and (b) chemical structure of CA were displayed. (c) cell viability was evaluated by cell counting kit-8 (CCK-8). (d) multiple nucleus giant cells (MNCs) were recognized as osteoclasts by TRAP staining. (e) the number of TRAP-positive MNCs and percentage of the TRAP-positive area were counted. (f) the secretions of inflammatory cytokines were measured by ELISA. * indicates $p < 0.05$, ** indicates $p < 0.01$.

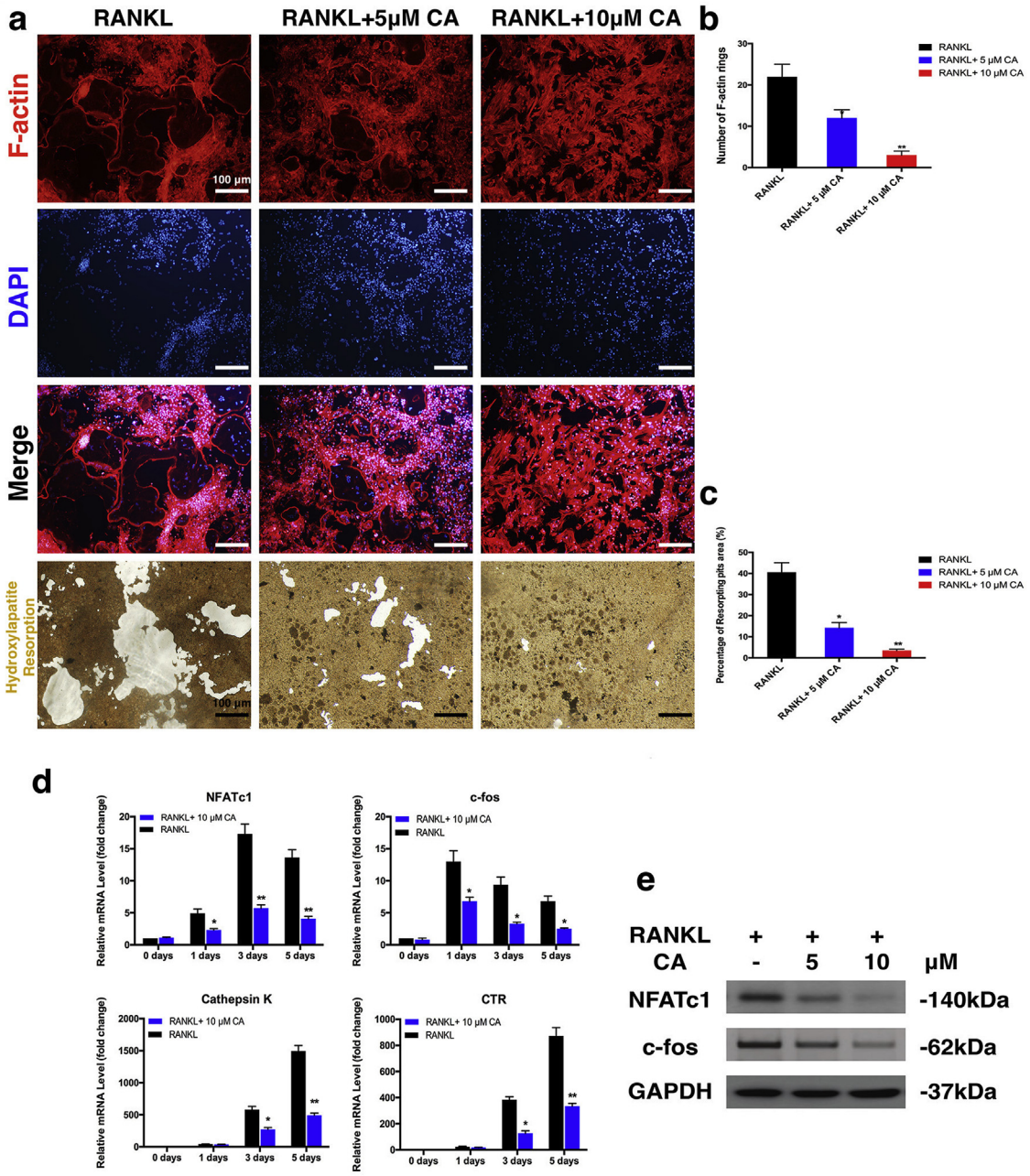

Fig. 2. CA inhibited the function of osteoclasts in vivo. (a,b) F-actin rings in osteoclasts were visualized by phalloidine/DAPI fluorescent staining and counted. (a,c) hydroxylapatite resorption by osteoclasts incubated with or without CA was evaluated. (d,e) osteoclastogenesis associated genes were investigated by RT-PCR and western blot. * indicates $p < 0.05$, ** indicates $p < 0.01$.

genes during osteoclast formation. Total mRNAs were extracted using Qiagen RNeasy Mini kit according to the manufacturer's instructions. cDNA was synthesized from 1 μg of total RNA using reverse transcriptase (TaKaRa Biotechnology, Otsu, Japan). Real-time PCR was performed using SYBR Premix Ex Taq kit (Takara) and an ABI 7500 Sequencing Detection System (Applied Biosystems, Foster City, CA, USA). The mouse primer sequences for NFATc1, c-fos, cathepsin K, calcitonin receptor (CTR) and GAPDH are listed in Table 1.

2.9. Western blotting analysis

Total proteins were isolated by centrifugation with 10000 *g* for 10 min after harvested cells lysed by radioimmunoprecipitation assay buffer (Beyotime, Shanghai, China) and 1% phenylmethylsulfonyl fluoride on ice for 30 min. Nuclear and cytoplasmic proteins were isolated and extracted as previously reported [27]. The concentrations of proteins were determined using a BCA kit (Thermo Pierce, Rockford, IL, USA). Protein bands were detected using an Odyssey V3.0 image scanner (Li-COR. Inc., Lincoln, NE, USA) after been dispersed in the SDS-PAGE gel by electrophoresis. The intensity of each band was analyzed using Image J software.

2.10. Immunofluorescent assay

4×10^3/dish RAW 264.7 cells were inoculated onto confocal dishes and incubated in serum-free media with or without a pretreatment of 10 μM CA or brusatol for starving 4 h. Then, all cells were stimulated with PBS or 50 ng/ml RANKL for 20 min before fixed by 4%

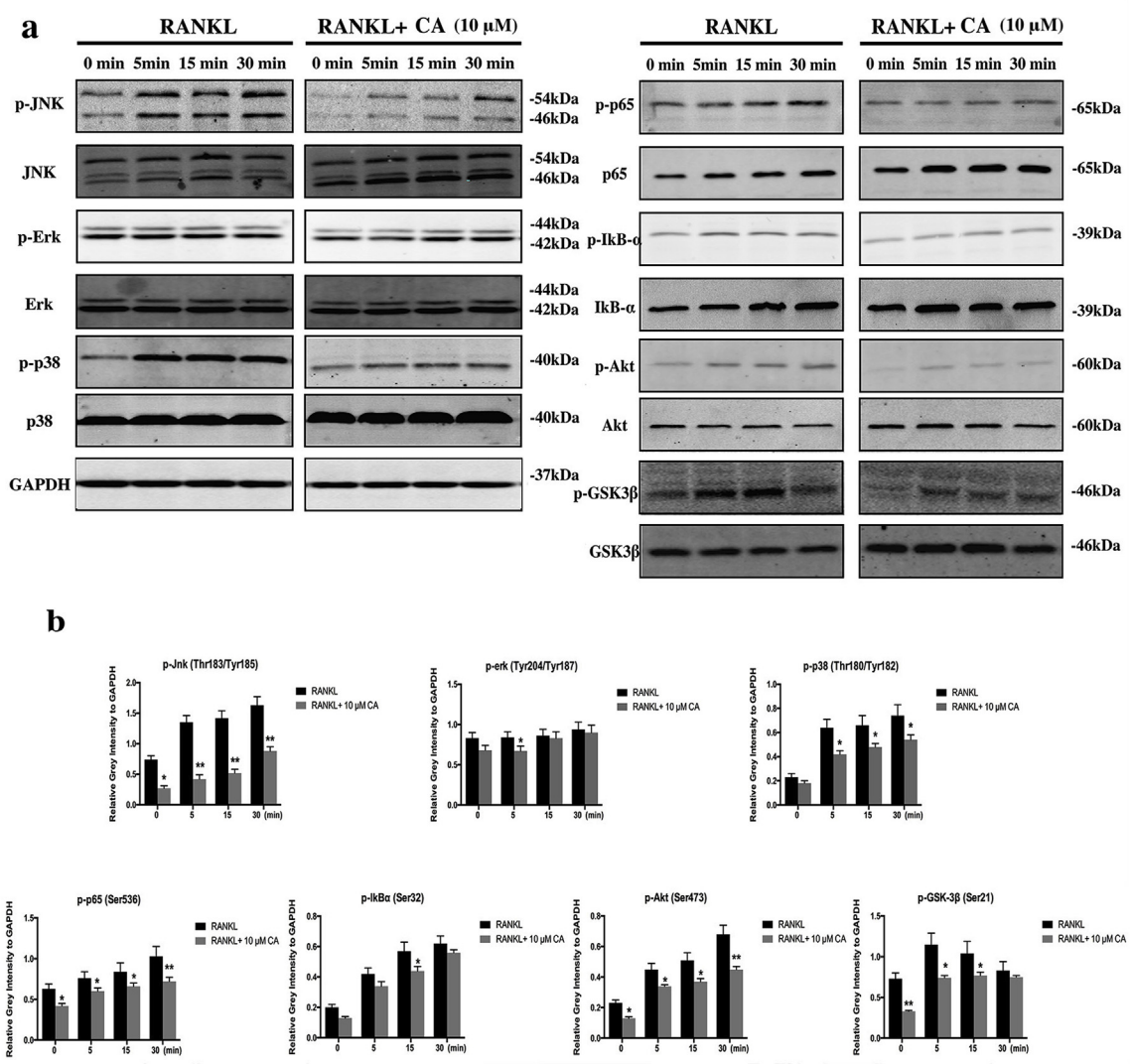

Fig. 3. The effect of 10 μM CA on the phosphorylation of MAPK, NF-κB, and Akt-GSK-3β pathway. (a) activations of JNK, ERK, p38, p65, IkBα, Akt, GSK-3β were detected by western blot. (b) Relative grey intensities were calculated. * indicates $p < 0.05$, ** indicates $p < 0.01$.

paraformaldehyde for 30 min, permeabilized by 0.1% Triton-100 for 5 min, and blocked by 10% BSA for 1 h. Eventually, cells were incubated with Anti-Nrf2 antibody conjugated with Alexa Fluor® 647 and observed under an LSM5 confocal microscope (Carl Zeiss, Oberkochen, Germany).

2.11. LPS-induced mouse calvarial osteolysis model and analysis

The Animal Care and Experiment Committee of Ninth People's Hospital, Shanghai Jiao Tong University School of Medicine approved all protocols. Thirty-two 8-week-old male mice were randomly separated into four groups: PBS (negative control), LPS (100 μg/day), LPS and low-dose CA (10 mg/kg/day), and LPS and high-dose CA (20 mg/kg/day). The calvarial osteolysis model was established by subcutaneously injecting 100 μg/day LPS onto calvaria on every other day for 2 weeks. On day 14, all mice were euthanized and calvaria was separated and fixed with 4% paraformaldehyde for 48 h.

Next, the calvaria were scanned by Micro-CT (μCT 80; SCANCO Medical AG, Bassersdorf, Switzerland) for bone morphometric analysis. When analyzing the middle-suture osteolysis area, the non-osseous tissue adjacent to and continuous with the midline suture was considered as the osteolysis area and this was analyzed using Image-Pro Plus 6.0 (Media Cybernetics; USA). For histological evaluations, calvaria were decalcified in 10% EDTA (pH 7.4) for 2 weeks and embedded in paraffin. Sectioned tissues were stained by hematoxylin and eosin (H&E) and TRAP staining. The average number of TRAP-positive multinucleated osteoclasts and the percentage of the TRAP-positive stained bone surface (OcS/BS, %) were calculated.

2.12. Immunohistochemistry analysis

Thereafter, tissue sections were de-waxed and dried followed by inhibiting endogenous peroxidases with 3% H2O2 and blocking non-specific antigens with 5% BSA. Then the tissue sections were incubated with primary antibodies against p-p65, p-JNK, and p-AMPK overnight at room temperature. Next day, tissue sections were incubated with polymerized peroxidase-labeled rabbit anti-mouse IgG and visualized by conventional DAB way.

2.13. Statistical analysis

The data in this study are displayed as the mean ± standard deviation (SD), and analyzed using SPSS 20.0 software (SPSS Inc., Chicago, IL, USA) and Prism 6 (GraphPad, La Jolla, CA, USA) by Student's t-test or one-way analysis of variance. $p < 0.05$ indicates statistical significance.

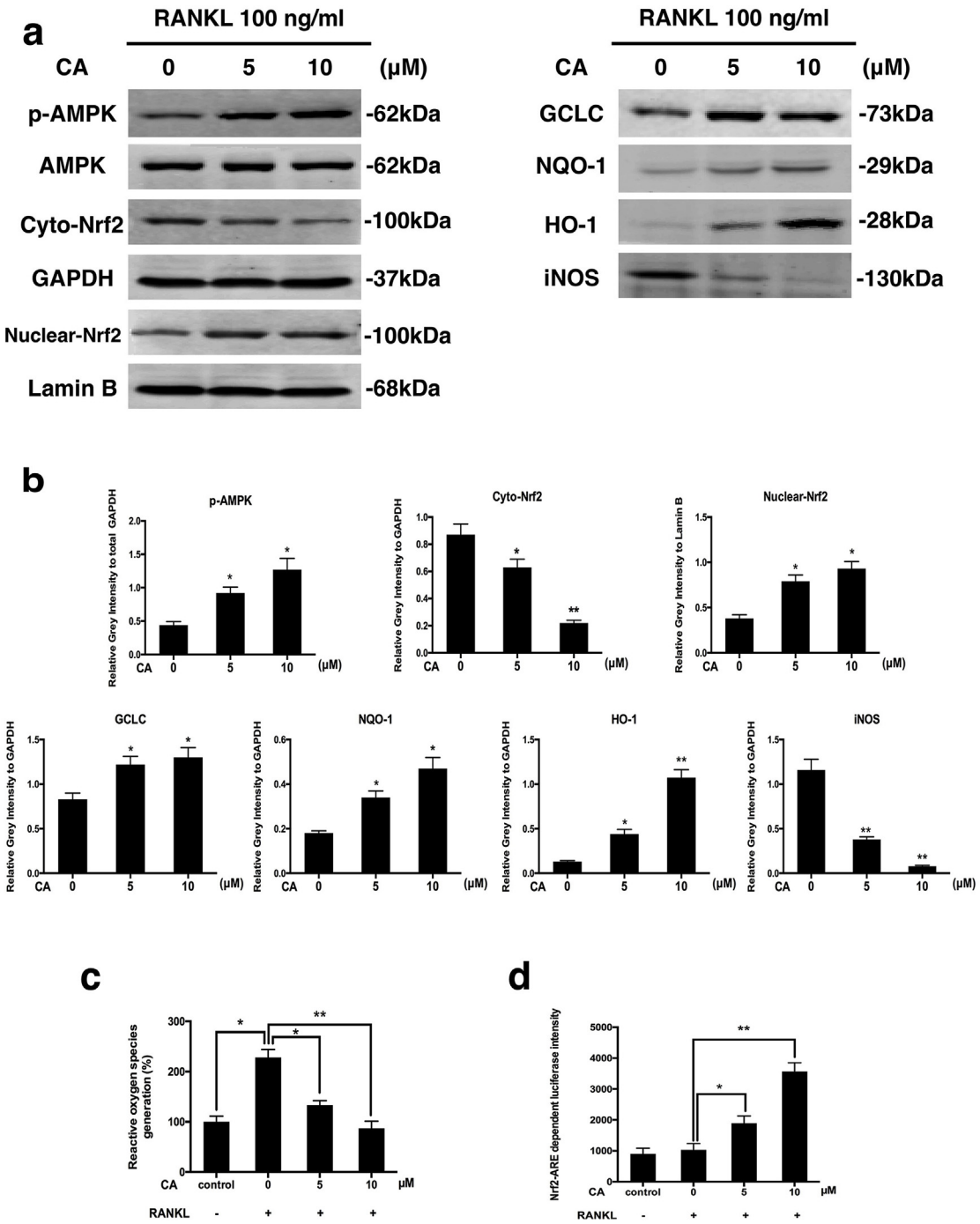

Fig. 4. The anti-oxidative effect of CA during its inhibiting osteoclastogenesis. (a,b) phosphorylation of AMPK and expression of Nrf2, HO-1, NQO-1, and GCLC were investigated by western blot. (c) Intracellular reactive oxygen species during RANKL-induced osteoclastogenesis with or without CA were detected. (d) The activity of Nrf2 was measured by luciferase assays. * indicates $p < 0.05$, ** indicates $p < 0.01$.

3. Results

3.1. CA inhibits RANKL-induced osteoclastogenesis and hydroxylapatite resorption by down-regulating NFATc1 and c-fos in vitro

The natural form and chemical structure of CA were displayed in Fig. 1 (a,b). Cell viabilities of RAW 264.7 cells and BMMs incubated with various concentrations of CA were detected using Cell Counting Kit-8 (CCK-8) at different times. As a result, CA with concentrations higher than 20 μM was demonstrated as a significant cytotoxicity on RAW 264.7 cells and BMMs (Fig. 1c). Therefore, 5 and 10 μM of CA without cytotoxicity were used in further study. The TRAP staining revealed that incubation with RANKL remarkably induced the formation of multiple nucleus giant cells fused by many monocytes. However, the number of MNCs and percentage of TRAP-positive stained area in the CA-treated group were both significantly less than those in the control group (Fig. 1d and e). Therefore, CA significantly suppressed RANKL-induced osteoclastogenesis in a time- and dose-dependent manner. Then, the inflammatory cytokines including TNF-α, IL-1β, and IL-6 in culture supernatant secreted by macrophages under the stimulation of LPS were evaluated by ELISA. All three factors in the LPS-stimulated group were much higher than the control group while

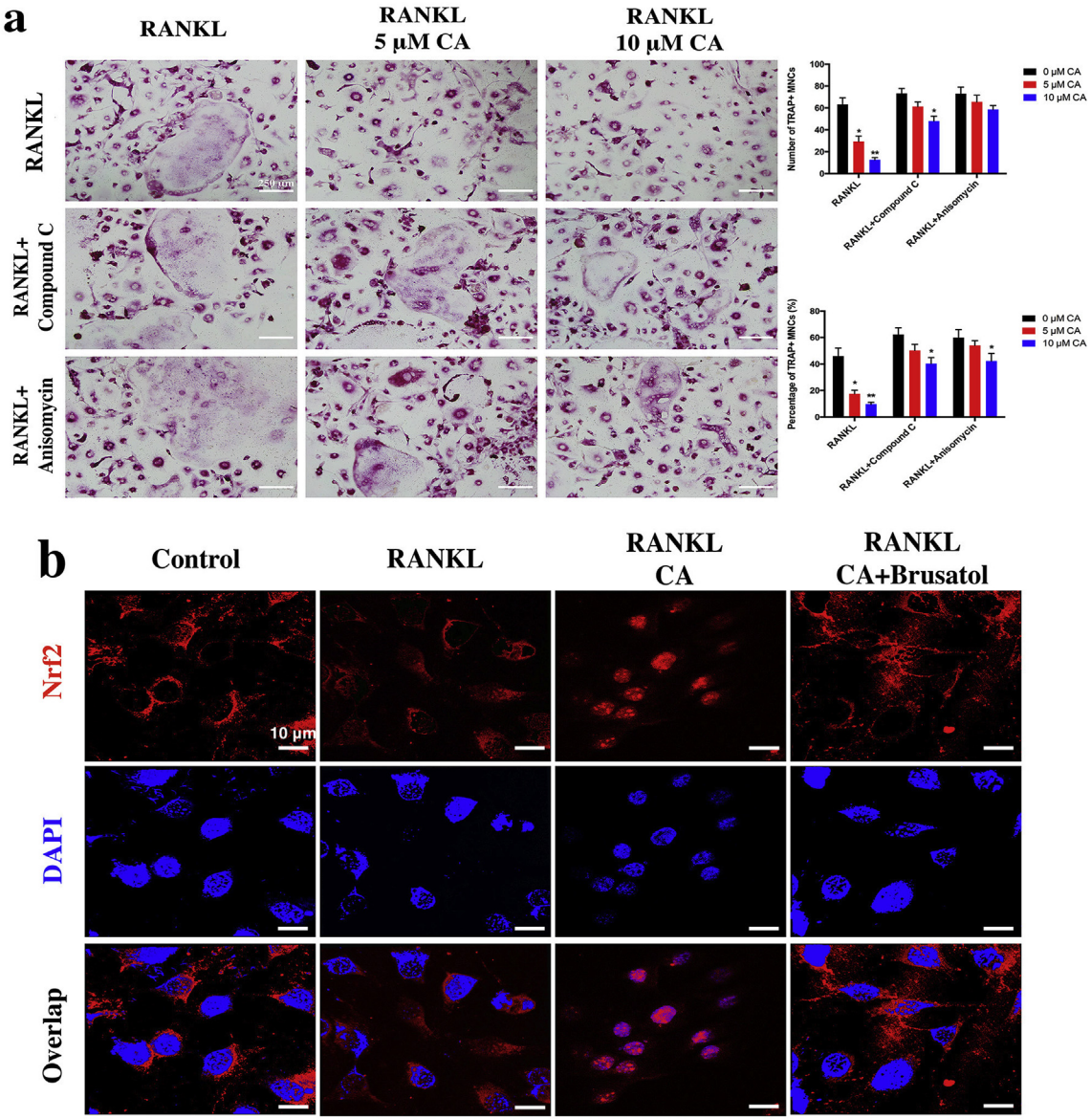

Fig. 5. 10 μM CA inhibited RANKL-induced osteoclastogenesis via inhibiting JNK and activating AMPK and Nrf2. (a) Anisomycin and Compound C used as an inhibitor of JNK and activator of AMPK respectively in the TRAP staining. (b) the translocation of Nrf2 in RANKL-stimulated cells was identified by immunofluorescent staining. * indicates $p < 0.05$, ** indicates $p < 0.01$.

remarkable lower than CA-treated group (Fig. 1f). We have also performed RT-PCR assays to detect the mRNA of COX-2 and iNOS in RAW 264.7 cells treated with PBS, LPS, LPS and 5 μM CA, or LPS and 10 μM CA for 0, 1, 3, and 5 d. It was observed that the expressions of COX-2 and iNOS dramatically increased in LPS-treated cells, while the increase was effectively inhibited by the treatment of CA (Fig. 1g).

Besides that the formation of osteoclasts was evaluated, the effect of CA on the function of osteoclasts was also estimated by F-actin ring staining and hydroxylapatite resorption assay. The number of F-actin ring in RANKL-induced mature osteoclasts was dramatically more than that in CA-treated osteoclasts (Fig. 2a and b). Meanwhile, much more pits were formed and hydroxylapatites were resorbed by osteoclasts in control group than CA-treated group (Fig. 2a,c). So it was suggested that CA inhibited the function of osteoclasts as well.

Next, the expressions of several osteoclastogenesis associated genes, such as NFATc1, c-fos, Cathepsin K and Calcitonin receptor (CTR), were investigated by RT-PCR and western blot. It was demonstrated that the mRNAs of NFATc1, c-fos, Cathepsin K, and CTR were down-regulated by CA by a time-dependent way (Fig. 2d). Meanwhile, the proteins of NFATc1 and c-fos in during RANKL-induced osteoclastogenesis were also inhibited by CA compared with control (Fig. 2e).

3.2. JNK was inhibited and AMPK-Nrf2 was activated by CA in RANKL-induced osteoclastogenesis

The activation of MAPK and NF-κB has been demonstrated as critical in RANKL-induced osteoclastogenesis by accumulative researches [8,28]. In our study, the active level of those kinases in the above two signal pathways were detected. As a result, RANKL-induced phosphorylation of JNK (p-JNK) was dramatically inhibited by CA. In addition, not as much as the inhibition of JNK, p-p38, p-p65, p-Akt, and p-GSK-3β were also inhibited in CA-treated cells, while p-ERK and p-IkBα were not obviously affected (Fig. 3a and b).

Since the intracellular oxidative stress and reactive oxygen species (ROS) have been demonstrated as contributors of RANKL-induced osteoclastogenesis [13,29,30], we subsequently analyzed the effect of CA on the activation of AMPK and Nrf2 (Fig. 4a and b). Consequently, it was observed that incubation of CA dose-dependently promoted the

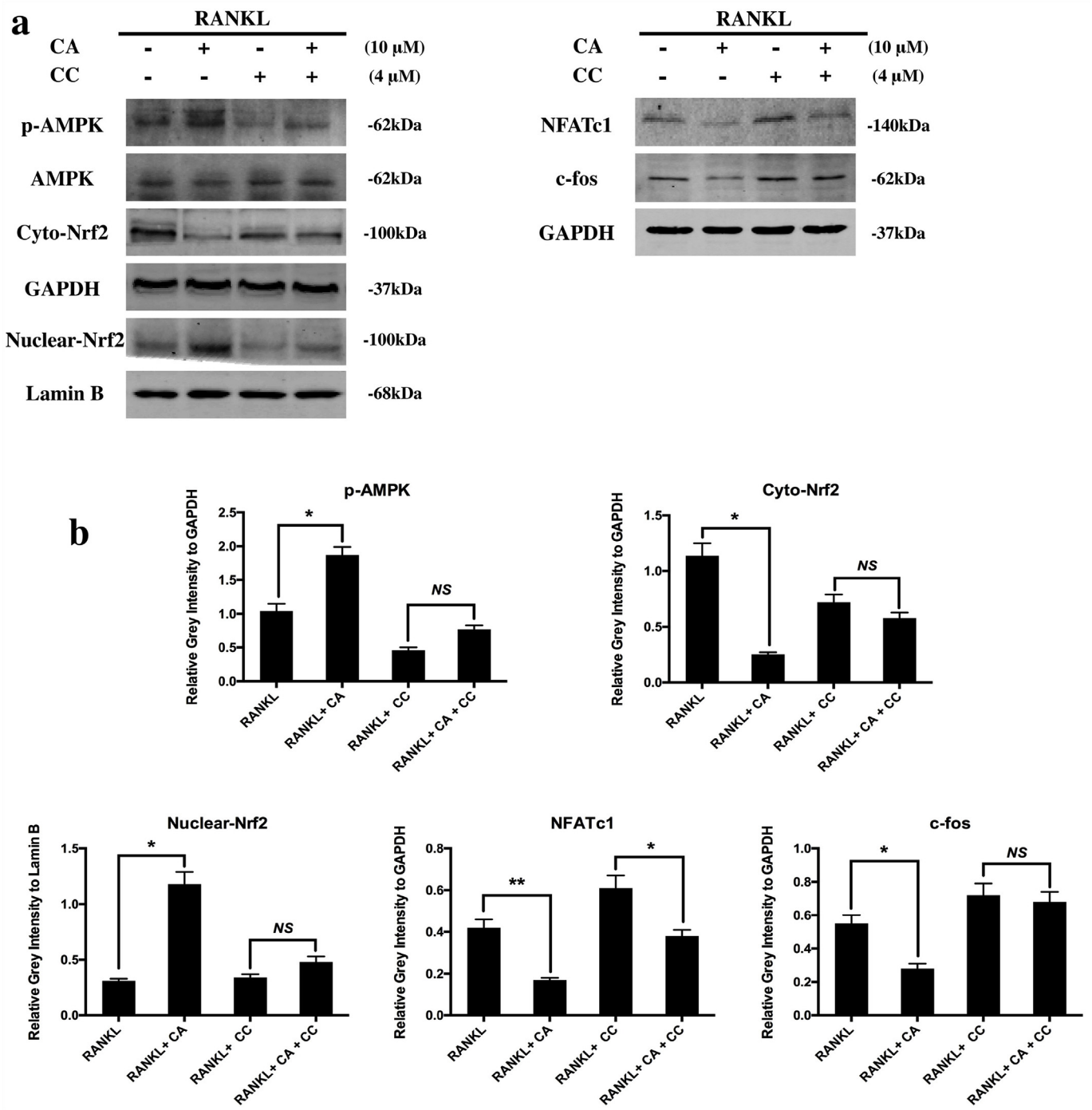

Fig. 6. The inhibition of p-AMPK rescued CA-induced activation of Nrf2 and antioxidants. (a) cytoplasmic and nuclear Nrf2 and its activated antioxidants were detected with or without Compound C or/and CA. (b) Relative grey intensities were calculated. * indicates $p < 0.05$, ** indicates $p < 0.01$.

phosphorylation of AMPK. Meanwhile, the expression of cytoplasmic Nrf2 was down-regulated while the expression of nuclear counterpart increased, indicating that Nrf2 was translocated into the nucleus from the cytoplasm to regulate downstream genes under the activation of CA. Moreover, several Nrf2-mediated anti-oxidative enzymes, including HO-1, NQO-1, and GCLC, were increased by CA during activation of Nrf2. As an inflammatory marker and producer of free radical, iNOS was inhibited by CA in RANKL-induced osteoclasts [31–33]. Next, the intracellular ROS was detected by Oxiselect™ Intracellular ROS assay kit (Cell Biolabs, Inc., San Diego, CA, USA). It was revealed that the ROS level in RANKL-stimulated cells was dramatically higher than the control group, but it was significantly reduced in CA-treated cells by a concentration-dependent way (Fig. 4c). A luciferase activity assay was used to further confirm the inhibitory effects of CA on Nrf2 (Fig. 4d). Our results showed that the transcription activity of Nrf2 was suppressed by CA in a concentration-dependent manner.

3.3. The effect of CA on p-JNK, p-AMPK, and Nrf2 was rescued by Anisomycin, Compound C, and Brusatol

For further demonstrated the above signaling mechanism of CA, Compound C (Dorsomorphin) and Anisomycin were used as the inhibitors of p-AMPK and activator of p-JNK in TRAP staining assays, respectively. As a result, the inhibitory effects of CA on both the number

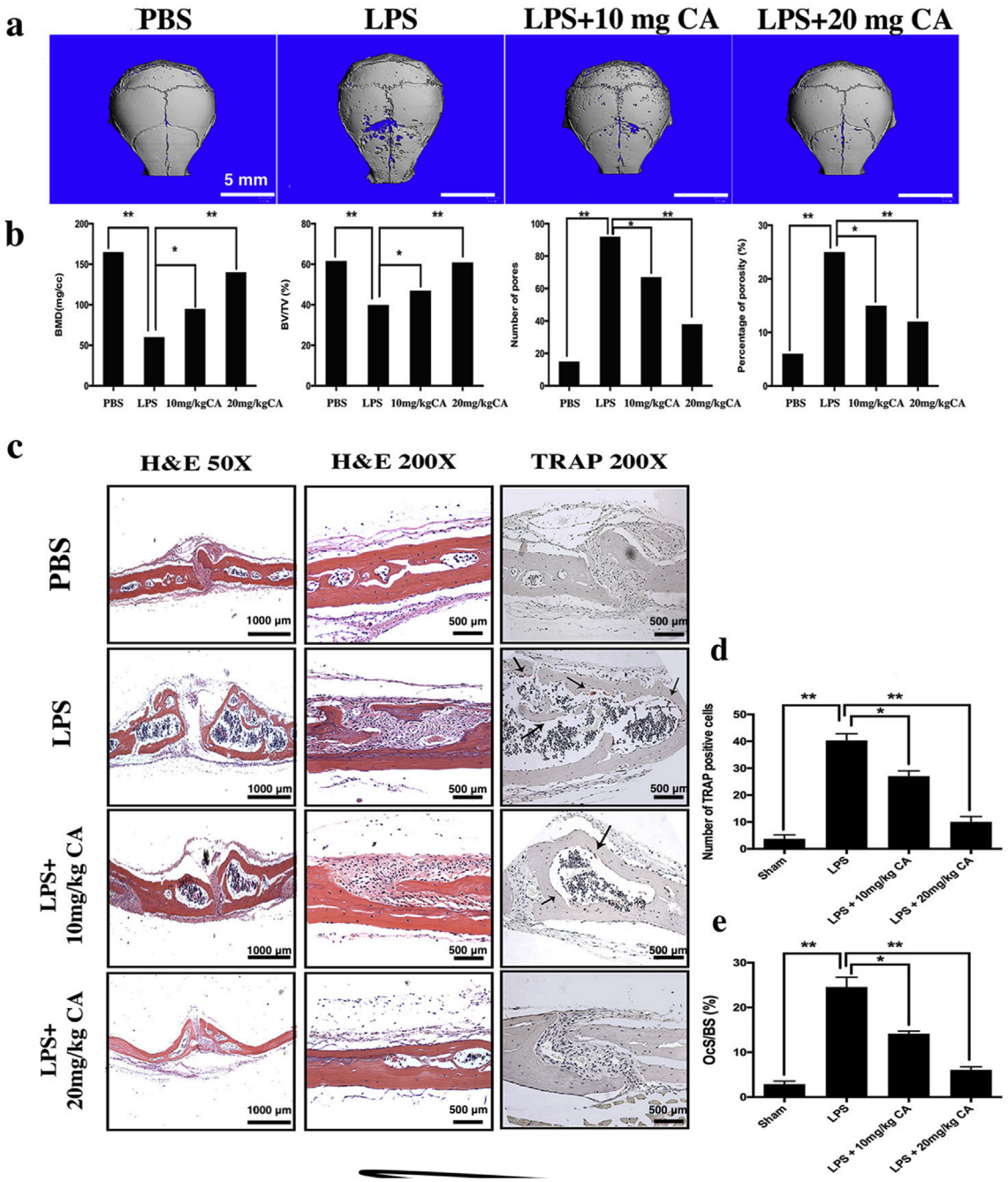

Fig. 7. CA inhibited LPS-induced mice calvaria osteolysis in vivo. (a) micro-CT was performed to evaluate the mice calvaria bone erosions. (b) BMD, BV/TV, number of pores, and the percentage of porosity were analyzed. (c) H&E and TRAP staining for histological evaluations. (d) the number of TRAP-positive cells and the percentage of the TRAP-positive area were calculated. * indicates $p < 0.05$, ** indicates $p < 0.01$.

of TRAP-positive stained MNCs and the percentage of the positive stained area were partially rescued in both CC and Anisomycin-treated groups in which p-AMPK and p-JNK were inhibited and activated, respectively (Fig. 5a). Moreover, Brusatol, an inhibitor targeting at Nrf2, was used in Nrf2 translocation assay. In immunofluorescent staining, Nrf2 was mainly located in the cytoplasm of RAW 264.7 cells with or without stimulation of RANKL. However, CA promoted the translocation of Nrf2 into the nucleus, which can be rescued by the addition of Brusatol (Fig. 5b).

Meanwhile, the activation of p-AMPK by CA was attenuated in CC-treated cells. According to the expressions of cyto-Nrf2 and Nuclear-Nrf2, it was demonstrated that CA-induced Nrf2 translocation was also inhibited by CC when p-AMPK was suppressed. The RANKL-induced expressions of NFATc1 and c-fos in CA-treated cells were decreased compared with controls, while CC restored these down-regulations (Fig. 6a and b).

3.4. CA ameliorated LPS-induced mice calvaria osteolysis in vivo

Histological assessment and histomorphometric analysis further confirmed that the treatment of CA protected against LPS-induced osteolysis. The LPS-induced mice calvarial osteolysis model was used to investigate the therapeutic effect of CA in vivo. According to the results of micro-CT scanning, remarkable more osteolytic lesions were formed in LPS-injected calvaria compared with the PBS group. But the treatment of CA successfully inhibited the LPS-induced osteolysis (Fig. 7a).

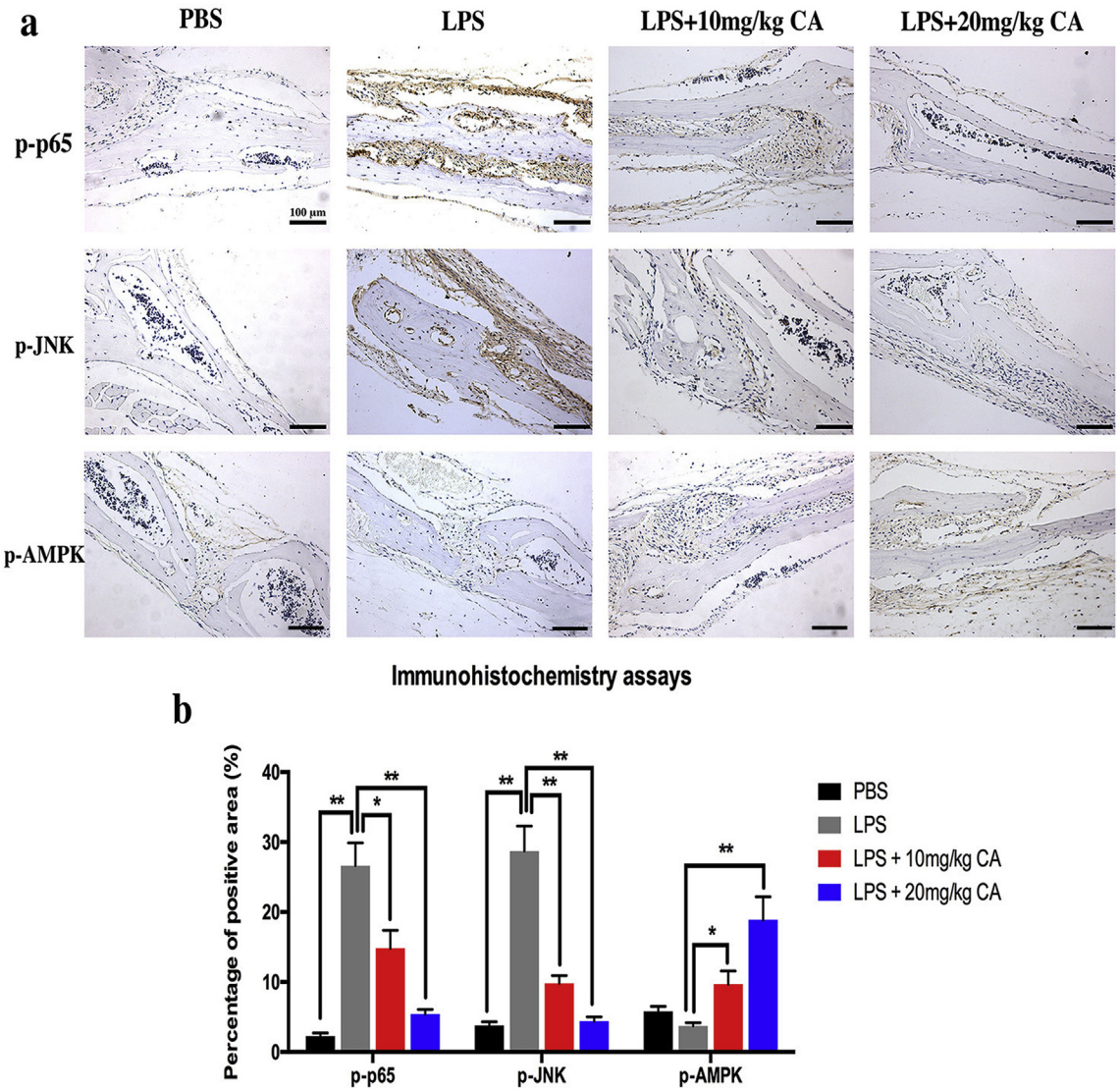

Fig. 8. CA inhibited p-p65 and p-JNK and activated p-AMPK in vivo. (a) immunohistochemistry assays were performed to investigate the effect of CA on kinases. (b) percentages of positive area of IHC were calculated and analyzed. * indicates $p < 0.05$, ** indicates $p < 0.01$.

The decreased BMD, BV/TV, number of pores, and percentage of porosity caused by LPS-induced inflammation were also correspondingly restored by the treatment of CA in bone-morphometric analyses (Fig. 7b). Obvious bone defects and inflammatory cells infiltration were observed in LPS-injected calvaria in H&E staining, while osteoclasia and inflammation were significantly disappeared in CA-treated groups (Fig. 7c).

TRAP staining revealed that the number of multinucleated osteoclasts (Black arrowheads) in the injection site was increased in response to the injection of LPS, which was indicated by the presence of osteoclasts that lined the eroded bone surface. However, in both the low- and high-concentration of CA-treated groups, the number of osteoclasts and the percentage of osteoclast surface relative to bone surface decreased (Fig. 7d and e), which indicates that CA inhibited osteoclast formation in LPS-induced osteolysis in vivo.

3.5. p-p65 and p-JNK were inhibited and p-AMPK was activated by the treatment of CA in vivo

In addition, immunohistochemistry assays were performed to further confirm the effect of CA on the kinases. As a result, p-p65 and p-JNK were highly activated in LPS-induced osteolysis group, but they were significantly inhibited in CA-injected mice. Moreover, the p-AMPK was remarkably higher expressed in CA-treated mice calvaria than those in PBS and LPS groups (Fig. a,b).

4. Discussion

The maintenance of normal bone mass largely depends on the homeostasis between the osteogenic effect of osteoblasts and the bone resorption activity of osteoclasts. Osteoclasts are multiple nucleus macrophages that are aggregated and fusion products of multiple monocytes that are stimulated by cytokines such as RANKL and TNF-α [34]. Recent studies on the molecular mechanisms of osteoclast differentiation and bone resorption-related genes and in-depth molecular mechanisms have revealed many new targets for effective treatment of osteoporosis. The drugs currently used in osteoporosis reduce bone resorption primarily by inhibiting osteoclast formation. Currently available antioxidants that are used include bisphosphonates, selective estrogen receptor modulators, calcitonin, and estrogen [35,36]. However, many recent studies have reported that some of these drugs cause serious health disorders such as breast cancer, endometritis, thromboembolism, hypercalcemia, osteonecrosis of the jaw, and atrial fibrillation [37,38]. Some plant-derived small-molecule compounds have

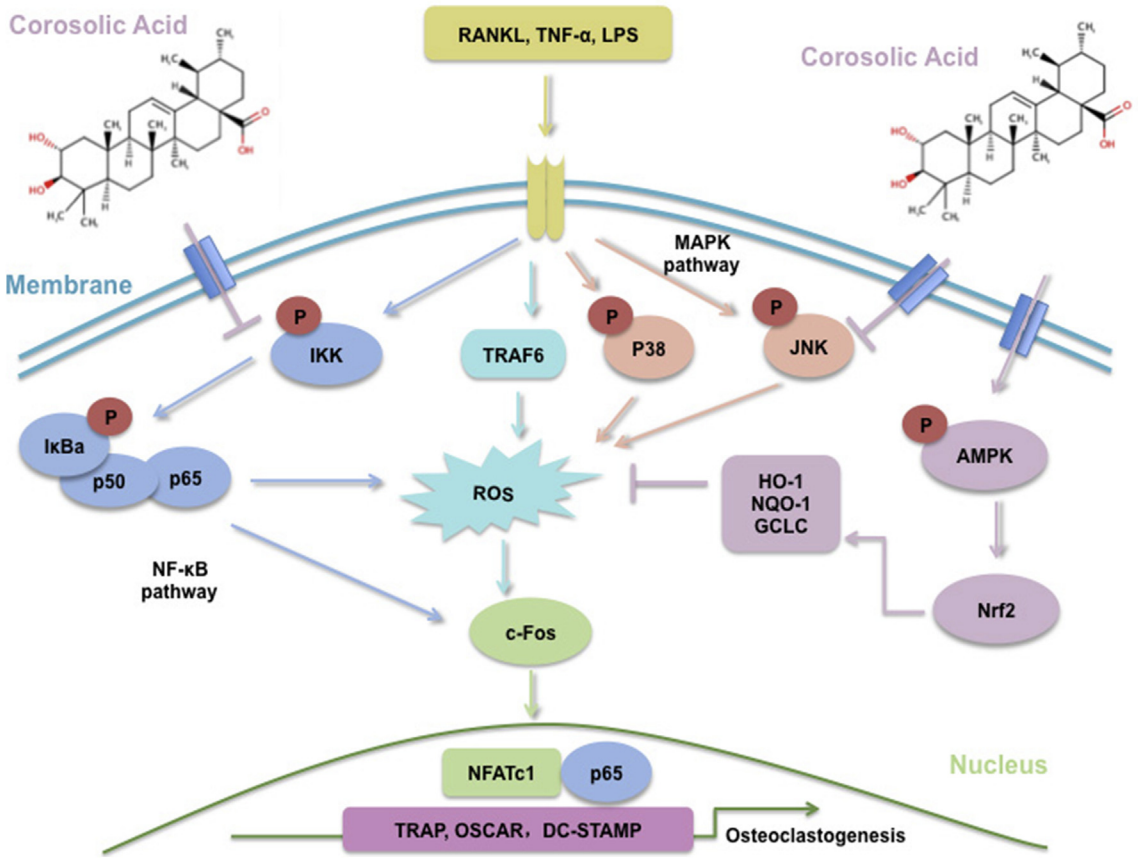

Fig. 9. Schematic of CA suppressing RANKL-induced osteoclastogenesis and oxidative stress. The phosphorylation of JNK and p65 were inhibited and the phosphorylation of AMPK was activated during the inhibition of CA, resulting in the translocation of Nrf2 and increases of antioxidants including HO-1, NQO-1, and GCLC.

also been used to inhibit osteoclast differentiation and bone resorption, because of their anti-inflammatory, antioxidant, anti-inflammatory, and antitumor effects [39–42]. CA has been previously reported as preventing mitochondrial fission by regulation of Drp1 phosphorylation (Ser637) in an AMPK-dependent manner, and blocking NOX2 oxidase signaling and suppressing NLRP3 inflammasome activation in the endothelium [43]. Meanwhile, CA ameliorates acute inflammation through inhibition of IRAK-1 phosphorylation in macrophages [44]. However, there is still no research about the effect of CA on osteoclastogenesis yet.

In the present study, we demonstrated that CA inhibited not only RANKL-induced maturation of osteoclasts (Fig. 1) but also functions of osteoclasts including the formation of F-actin rings and hydroxylapatite resorption in vitro (Fig. 2). The critical genes regulating osteoclastogeneses, such as NFATc1, c-fos, Cathepsin K, and CTR, were significantly inhibited by CA during the RANKL-induced osteoclastogenesis (Fig. 2). Additionally, an LPS-stimulated inflammatory model was established using RAW 264.7 cells to evaluated the anti-inflammation property of CA. It was observed that CA dose-dependently decreased the LPS-stimulated secretions of TNF-α, IL-1β, and IL-6 (Fig. 1). Meanwhile, LPS-induced increase of inflammatory markers, including COX-2 and iNOS, were attenuated by the treatment of CA. Moreover, Balakrishnan and Al-Assaf recently has reported that the mRNA levels of several proinflammatory cytokines or markers including TNF-α, IL-6, iNOS, and COX-2 and NF-kB signaling pathway were significantly up regulated in CCl(4) induced rats and treatment with corosolic acid significantly reduced the expression of the above indicators [45]. As NF-κB and MAPK were critical signaling pathways in osteoclastogenesis, the phosphorylations of these kinases in cells treated by CA were detected. Our results indicate that p-JNK was dramatically inhibited by CA. Besides, p-p38, p-p65, p-Akt, and p-GSK-3β were partly suppressed by CA as well, although not as much as p-JNK (Fig. 3). Therefore, it was demonstrated that CA inhibited LPS-induced inflammation and RANKL-induced osteoclastogenesis via down-regulating p-JNK. Furthermore, CA activated p-AMPK during the RANKL-induced formation of osteoclasts (Fig. 4a). Yang et al. reported that Corosolic acid inhibits adipose tissue inflammation and ameliorates insulin resistance via AMPK activation in high-fat-fed mice, which is consistent with our results.

Since ROS and oxidative stress also contribute to formation and function of osteoclasts, we subsequently evaluated the effect of CA on intracellular ROS of osteoclasts [46,47]. It was observed that in RANKL-stimulated cells cytoplasmic Nrf2 was decreased and nuclear Nrf2 was increased after treatment with CA. Accordingly, several Nrf2-mediated antioxidants including HO-1, NQO-1, and GCLC were also up-regulated by CA. our research showed that RANKL dramatically increased the intracellular ROS level that, however, was concentration-dependently inhibited by CA (Fig. 4). To further verify the mechanism of CA during its inhibiting RANKL-induced osteoclastogenesis, Compound C and Anisomycin were used as inhibitor and activator of p-AMPK and p-JNK, respectively. Then, the inhibitory effect of CA on RANKL-induced osteoclastogenesis was significantly rescued at both CC and Anisomycin treated cells. Moreover, the CA-induced translocation of Nrf2 was visualized in immunofluorescent assays. CA clearly promoted the Nrf2 translocating from cytoplasm to nucleus, which, however, was attenuated by the addition of Brusatol, an inhibitor of Nrf2 (Fig. 5). Taken together, CA suppressed RANKL-induced osteoclastogenesis via inhibiting JNK and activating AMPK-Nrf2 axis. Guo et al. previously demonstrated that CA significantly inhibited ethanol-caused intracellular accumulation of ROS in vitro and ethanol-activated phosphorylation of p38 and JNK both in vitro and in vivo [48]. They also found that

ethanol-caused down-regulation of autophagy associated genes, such as beclin-1 and LCII/I, were attenuated by CA through activating AMPK. Li et al. reported that the activation of ERK and p38 were both suppressed by CA in diabetic mice and glomerular mesangial cells [41].

We also investigated the therapeutic effect of CA in LPS-induced mice calvarial osteolysis model. The bone-morphometric analysis demonstrated that the LPS-induced osteolysis model was successfully established with remarkable bone erosion area in micro-CT scanning, and these bone losses were significantly inhibited by the treatment of CA. Meanwhile, the highly bone destruction and osteoclastogenesis in LPS group were also dose-dependently attenuated in CA-treated groups (Fig. 7). p-p65 and p-JNK were highly activated in LPS-injected mice calvaria by immunohistochemistry analyses, while they were inhibited by CA. It was also observed that CA activated p-AMPK during its inhibiting LPS-induced osteolysis in vivo, which is consistent with our in vitro results (Fig. 8).

In conclusion, our study firstly reported that CA effectively inhibited RANKL-induced osteoclastogenesis and oxidative stress in vitro and LPS-induced mice calvarial osteolysis. Further investigation demonstrated that osteoclastogenesis associated genes including NFATc1, c-fos, cathepsin K, and CTR were suppressed via inhibiting p-JNK and activating p-AMPK-Nrf2 by CA (Fig. 9). Therefore, CA can be used for treating osteolysis disorders such as osteoporosis, osteoarthritis, and prosthetic aseptic loosening. However, further studies are required for evaluating the safety and efficacy of this drug and examining its effects in large animal models and clinical trials.

Disclosure

The authors have declared that no competing interests exist.

Acknowledgments

The study was supported by National Natural Science Foundation of China (Grant No. 81772326) and National Key R&D Program of China (2018YFB1105600). We appreciate the kind support and help from the whole staff of Shanghai Key Laboratory of Orthopaedic Implants.

References

[1] G. Brunetti, P. D'Amelio, M. Wasniewska, G. Mori, M.F. Faienza, Editorial: bone: endocrine target and organ, Front. Endocrinol. 8 (2017) 354.
[2] S.L. Dallas, P.A. Veno, Live imaging of bone cell and organ cultures, Methods Mol. Biol. 816 (2012) 425–457.
[3] S.E. Hong, et al., Euphorbia factor L1 inhibits osteoclastogenesis by regulating cellular redox status and induces Fas-mediated apoptosis in osteoclast, Free Radic. Biol. Med. 112 (2017) 191–199.
[4] A.D. Leung, D. Yamanouchi, Osteoclastogenesis in abdominal aortic aneurysms: a new therapeutic target, Curr. Drug Targets 19 (11) (2018) 1233–1240, https://doi.org/10.2174/1389450118666170925155044.
[5] B.G. Matthews, et al., Splenomegaly, myeloid lineage expansion and increased osteoclastogenesis in osteogenesis imperfecta murine, Bone 103 (2017) 1–11.
[6] Y. Jiang, et al., Oxymatrine exerts protective effects on osteoarthritis via modulating chondrocyte homoeostasis and suppressing osteoclastogenesis, J. Cell Mol. Med. (2018 May 25), https://doi.org/10.1111/jcmm.13674 [Epub ahead of print].
[7] X. Chen, et al., 18beta-Glycyrrhetinic acid inhibits osteoclastogenesis in vivo and in vitro by blocking RANKL-mediated RANK-TRAF6 interactions and NF-kappaB and MAPK signaling pathways, Front. Pharmacol. 9 (2018) 647.
[8] C. Li, et al., Maslinic acid suppresses osteoclastogenesis and prevents ovariectomy-induced bone loss by regulating RANKL-mediated NF-kappaB and MAPK signaling pathways, J. Bone Miner. Res. 26 (3) (2011) 644–656.
[9] N.K. Lee, et al., A crucial role for reactive oxygen species in RANKL-induced osteoclast differentiation, Blood 106 (3) (2005) 852–859.
[10] P.G. Wells, et al., Oxidative stress in developmental origins of disease: teratogenesis, neurodevelopmental deficits, and cancer, Toxicol. Sci. 108 (1) (2009) 4–18.
[11] H. Esterbauer, R.J. Schaur, H. Zollner, Chemistry and biochemistry of 4-hydroxynonenal, malonaldehyde and related aldehydes, Free Radic. Biol. Med. 11 (1) (1991) 81–128.
[12] T.W. Kensler, N. Wakabayashi, S. Biswal, Cell survival responses to environmental stresses via the Keap1-Nrf2-ARE pathway, Annu. Rev. Pharmacol. Toxicol. 47 (2007) 89–116.
[13] H. Kanzaki, et al., Nuclear Nrf2 induction by protein transduction attenuates osteoclastogenesis, Free Radic. Biol. Med. 77 (2014) 239–248.
[14] H. Kanzaki, et al., Molecular regulatory mechanisms of osteoclastogenesis through cytoprotective enzymes, Redox Biol 8 (2016) 186–191.
[15] N. Wakabayashi, S.L. Slocum, J.J. Skoko, S. Shin, T.W. Kensler, When NRF2 talks, who's listening? Antioxidants Redox Signal. 13 (11) (2010) 1649–1663.
[16] M.K. Hasan, et al., Alpha-7-nicotinic acetylcholine receptor agonist ameliorates nicotine plus high-fat diet-induced hepatic steatosis in male mice by inhibiting oxidative stress and stimulating AMPK signaling, Endocrinology 159 (2) (2018 Feb 1) 931–944, https://doi.org/10.1210/en.2017-00594.
[17] R. Kumar, et al., Procyanidin B2 3,3"-di-O-gallate induces oxidative stress-mediated cell death in prostate cancer cells via inhibiting MAP kinase phosphatase activity and activating ERK1/2 and AMPK, Mol. Carcinog. 57 (1) (2018) 57–69.
[18] X. Zhou, et al., Serine prevented high-fat diet-induced oxidative stress by activating AMPK and epigenetically modulating the expression of glutathione synthesis-related genes, Biochim. Biophys. Acta 1864 (2) (2018) 488–498.
[19] G.G. Pellegrini, C.C. Morales, T.C. Wallace, L.I. Plotkin, T. Bellido, Avenanthramides prevent osteoblast and osteocyte apoptosis and induce osteoclast apoptosis in vitro in an Nrf2-independent manner, Nutrients 8 (7) (2016).
[20] D. Thummuri, V.G.M. Naidu, P. Chaudhari, Carnosic acid attenuates RANKL-induced oxidative stress and osteoclastogenesis via induction of Nrf2 and suppression of NF-kappaB and MAPK signalling, J. Mol. Med. (Berl.) 95 (10) (2017) 1065–1076.
[21] K.S. Ahn, M.S. Hahm, E.J. Park, H.K. Lee, I.H. Kim, Corosolic acid isolated from the fruit of Crataegus pinnatifida var. psilosa is a protein kinase C inhibitor as well as a cytotoxic agent, Planta Med. 64 (5) (1998) 468–470.
[22] Y. Xu, et al., Corosolic acid induces apoptosis through mitochondrial pathway and caspase activation in human cervix adenocarcinoma HeLa cells, Cancer Lett. 284 (2) (2009) 229–237.
[23] J. Yang, et al., Corosolic acid inhibits adipose tissue inflammation and ameliorates insulin resistance via AMPK activation in high-fat fed mice, Phytomedicine 23 (2) (2016) 181–190.
[24] C. Wang, et al., Sitagliptin, an anti-diabetic drug, suppresses estrogen deficiency-induced OsteoporosisIn vivo and inhibits RANKL-induced osteoclast formation and bone resorption in vitro, Front. Pharmacol. 8 (2017) 407.
[25] X.Z. Zeng, et al., Aconine inhibits RANKL-induced osteoclast differentiation in RAW264.7 cells by suppressing NF-kappaB and NFATc1 activation and DC-STAMP expression, Acta Pharmacol. Sin. 37 (2) (2016) 255–263.
[26] J. Jin, et al., Role of Nrf2 activation and NF-kappaB inhibition in valproic acid induced hepatotoxicity and in diammonium glycyrrhizinate induced protection in mice, Food Chem. Toxicol. 73 (2014) 95–104.
[27] K. Ito, E. Jazrawi, B. Cosio, P.J. Barnes, I.M. Adcock, p65-activated histone acetyltransferase activity is repressed by glucocorticoids: mifepristone fails to recruit HDAC2 to the p65-HAT complex, J. Biol. Chem. 276 (32) (2001) 30208–30215.
[28] H. Wu, et al., Artemether attenuates LPS-induced inflammatory bone loss by inhibiting osteoclastogenesis and bone resorption via suppression of MAPK signaling pathway, Cell Death Dis. 9 (5) (2018) 498.
[29] H. Kim, Y.D. Lee, H.J. Kim, Z.H. Lee, H.H. Kim, SOD2 and Sirt3 control osteoclastogenesis by regulating mitochondrial ROS, J. Bone Miner. Res. 32 (2) (2017) 397–406.
[30] H. Kanzaki, F. Shinohara, M. Kajiya, T. Kodama, The Keap1/Nrf2 protein axis plays a role in osteoclast differentiation by regulating intracellular reactive oxygen species signaling, J. Biol. Chem. 288 (32) (2013) 23009–23020.
[31] K. Stadler, et al., Direct evidence of iNOS-mediated in vivo free radical production and protein oxidation in acetone-induced ketosis, Am. J. Physiol. Endocrinol. Metab. 295 (2) (2008) E456–E462.
[32] M. Bagheri, R.R. Nair, K.K. Singh, D.K. Saini, ATM-ROS-iNOS axis regulates nitric oxide mediated cellular senescence, Biochim. Biophys. Acta 1864 (1) (2017) 177–190.
[33] A. Kumar, et al., iNOS polymorphism modulates iNOS/NO expression via impaired antioxidant and ROS content in P. vivax and P. falciparum infection, Redox Biol 15 (2018) 192–206.
[34] A. Dharmapatni, et al., Osteoclast-associated Receptor (OSCAR) Distribution in the Synovial Tissues of Patients with Active RA and TNF-alpha and RANKL Regulation of Expression by Osteoclasts in Vitro. Inflammation, (2017).
[35] C. Chakraborty, C.G. Doss, Crucial protein based drug targets and potential inhibitors for osteoporosis: new hope and possibilities, Curr. Drug Targets 14 (14) (2013) 1707–1713.
[36] C. Deal, Potential new drug targets for osteoporosis, Nat. Clin. Pract. Rheumatol. 5 (1) (2009) 20–27.
[37] B. Xu, D. Lovre, F. Mauvais-Jarvis, The effect of selective estrogen receptor modulators on type 2 diabetes onset in women: basic and clinical insights, J. Diabet. Complicat. 31 (4) (2017) 773–779.
[38] F.Y. Hsiao, W.W. Hsu, Comparative risks for cancer associated with use of calcitonin, bisphosphonates or selective estrogen receptor modulators among osteoporosis patients: a population-based cohort study, Jpn. J. Clin. Oncol. 47 (10) (2017) 935–941.
[39] H.O.B. Oloyede, H.O. Ajiboye, M.O. Salawu, T.O. Ajiboye, Influence of oxidative stress on the antibacterial activity of betulin, betulinic acid and ursolic acid, Microb. Pathog. 111 (2017) 338–344.
[40] W. Zhou, L. Lin, Y. Cheng, Y. Liu, Ursolic acid improves liver transplantation and inhibits apoptosis in miniature pigs using donation after cardiac death, Cell. Physiol. Biochem. 43 (1) (2017) 331–338.
[41] X.Q. Li, et al., Corosolic acid inhibits the proliferation of glomerular mesangial cells and protects against diabetic renal damage, Sci. Rep. 6 (2016) 26854.
[42] W. Zhao, et al., Metformin and resveratrol ameliorate muscle insulin resistance through preventing lipolysis and inflammation in hypoxic adipose tissue, Cell. Signal. 28 (9) (2016) 1401–1411.
[43] Y. Li, et al., Inhibition of mitochondrial fission and NOX2 expression prevent NLRP3

inflammasome activation in the endothelium: the role of corosolic acid action in the amelioration of endothelial dysfunction, Antioxidants Redox Signal. 24 (16) (2016) 893–908.
[44] S.J. Kim, et al., Corosolic acid ameliorates acute inflammation through inhibition of IRAK-1 phosphorylation in macrophages, BMB Rep 49 (5) (2016) 276–281.
[45] A.A.-A.A. Balakrishnan, Corosolic acid suppresses the expression of inflammatory marker genes in CCL4-induced-hepatotoxic rats, Pak. J. Pharm. Sci. 29 (4) (2016) 1133–1138.
[46] K. Nishimura, et al., TRAP-positive osteoclast precursors mediate ROS/NO-dependent bactericidal activity via TLR4, Free Radic. Biol. Med. 97 (2016) 330–341.
[47] S. Hyeon, H. Lee, Y. Yang, W. Jeong, Nrf2 deficiency induces oxidative stress and promotes RANKL-induced osteoclast differentiation, Free Radic. Biol. Med. 65 (2013) 789–799.
[48] X. Guo, et al., Corosolic acid protects hepatocytes against ethanol-induced damage by modulating mitogen-activated protein kinases and activating autophagy, Eur. J. Pharmacol. 791 (2016) 578–588.